Spatial Patterns of Energy-Related Carbon Emissions from Residential Land: A Hybrid Physics-Machine Learning Study of Shenzhen

Lingyun Yao , Yonglin Zhang * , Ke Wang , Bo Huang , Zheng Niu , Li Wang *

Posted Date: 24 March 2026

doi: 10.20944/preprints202603.1914.v1

Keywords: hybrid modelling; building energy use; operational CO2 emissions; downscaling allocation

 doi:10.20944/preprints202603.1914.v1

Article

Spatial Patterns of Energy-Related Carbon Emissions from Residential Land: A Hybrid Physics-Machine Learning Study of Shenzhen

Lingyun Yao [1,2], Yonglin Zhang [1,*], Ke Wang [3], Bo Huang [4], Zheng Niu [1,2] and Li Wang [1,*]

[1] State Key Laboratory of Remote Sensing and Digital Earth, Aerospace Information Research Institute, Chinese Academy of Sciences, Beijing, China
[2] University of Chinese Academy of Sciences, Beijing, China
[3] School of Land Science and Technology, China University of Geosciences, Beijing, China
[4] Department of Geography, The University of Hong Kong, Hong Kong, China
* Correspondence: zhangyonglin@aircas.ac.cn (Y.Z.), wangli@aircas.ac.cn (L.W.)

Abstract

Accurate estimation of residential building energy consumption and energy-related carbon emissions is essential for supporting urban low-carbon development. This study proposes a hybrid modelling framework that integrates physics-based simulation and machine learning to estimate residential building energy use in Shenzhen for 2020. Representative building archetypes are simulated, and the results are used to train machine learning models for large-scale application. A bottom-up inventory combined with spatial-proxy-based downscaling is further employed to generate high spatiotemporal resolution maps of carbon emissions. Results show that the model achieves strong estimation performance across multiple scales. Daily mean temperature is the dominant driver of energy-use variability, while building type significantly influences consumption levels. Residential energy use is generally higher on weekends than weekdays. Spatially, emissions are concentrated in central and western districts, with Longgang having the highest emissions (11.19 Mt), followed by Bao'an, Longhua, and Nanshan. High-emission buildings are mainly located along road-adjacent areas. The proposed framework provides a robust and scalable approach for fine-resolution CO_2 emission estimation and supports accurate emission source attribution for urban carbon management.

Keywords: hybrid modelling; building energy use; operational CO_2 emissions; downscaling allocation

1. Introduction

In 2022, the total energy consumption from building operation and the construction sector in China reached 2.42 billion tonnes of standard coal equivalent (tce), accounting for 44.8% of the national total energy consumption. According to the report released by the China Association of Building Energy Efficiency, associated CO_2 emissions amounted to 5.13 billion tonnes of CO_2, representing 48.3% of the country's energy-related CO_2 [1,2]. China has pledged to achieve carbon peaking by 2030 and carbon neutrality by 2060. The building sector therefore holds considerable potential for carbon reduction, with an estimated 30% of emissions economically and efficiently reducible [3]. The reconstruction and fine-scale mapping of building operational energy consumption and emissions at high spatiotemporal resolution are crucial for formulating and implementing effective energy-saving and emission-reduction strategies [4,5], thereby providing essential support for achieving the twin goals [6].

Fine resolution CO_2 emission inventories and mapping play a critical role in precisely identifying dominant emission sources, enabling differentiated monitoring of CO_2 emissions, and

 doi:10.20944/preprints202603.1914.v1

supporting targeted carbon-reduction strategies. Despite the growing demand for fine-resolution and long-term urban building energy and CO_2 emissions datasets in research and regulatory practice, such data remain largely unavailable [7,8]. Specifically, historical building operational energy data and fine-resolution operational CO_2 emissions datasets are severely lacking at the city scale [9].

The bottom-up inventory approach is the carbon emission accounting method recommended by the IPCC guidelines. It estimates emissions based on statistics at the level of specific emission sources or activities, calculating carbon emissions using emission factors and activity data, and then aggregating them step by step to obtain the total emission results[10]. The spatialization of bottom-up carbon emission inventories derived from activity data is generally conducted through spatial downscaling based on spatial proxy data. Such proxy datasets generally represent spatial patterns of human activities and energy consumption intensity, including population distribution, mobile phone signalling data, and taxi trajectory records. In recent years, satellite-derived nighttime light data have also been widely validated as effective proxies for spatially allocating emissions. Representative top-down emission inventory systems include the Emissions Database for Global Atmospheric Research (EDGAR) [11] and the Open-Data Inventory for Anthropogenic Carbon dioxide (ODIAC) [12].

However, due to the relatively long update cycles of statistical yearbook data, top-down approaches often struggle to satisfy the requirements for high spatiotemporal resolution estimation and analysis of building energy consumption and CO_2 emissions [13]. In addition, considerable uncertainties arise in urban-scale applications [14,15], largely because these approaches depend heavily on proxy data for spatial allocation [4]. Consequently, the accuracy and representativeness of proxy datasets fundamentally constrain the reliability of top-down methods at finer spatial scales.

With the deepening advancement of China's carbon peaking and carbon neutrality goals, policy frameworks have increasingly emphasized dual constraints on both the total volume and intensity of carbon emissions, thereby placing higher demands on the refined management of carbon emissions. This research proposes a novel approach for generating fine-resolution spatiotemporal proxy data. By integrating physics-based modelling with machine learning techniques within a hybrid framework, the approach enables daily building-level estimation of energy consumption. The resulting proxy data are subsequently employed for fine-resolution spatiotemporal downscaling and allocation of CO_2 emissions within the building sector. This approach effectively overcomes the limitations in spatiotemporal resolution commonly encountered in city-scale carbon emission studies, thereby enabling more refined emission representation and supporting carbon emission management in urban areas characterized by complex land-use patterns.

2. Materials and Methods

2.1. Study Area and Data Source

The study area is located in Shenzhen, Guangdong Province, China, which is characterized by a subtropical monsoon climate with mild winters, hot summers, and abundant precipitation. Shenzhen has a highly developed economy, and the strong concentration of population and economic activities has contributed to the growth of residential CO_2 emissions. Meanwhile, as one of China's first national low-carbon pilot cities, Shenzhen holds significant demonstrative value in carbon emission monitoring and the implementation of carbon reduction policies.

 doi:10.20944/preprints202603.1914.v1

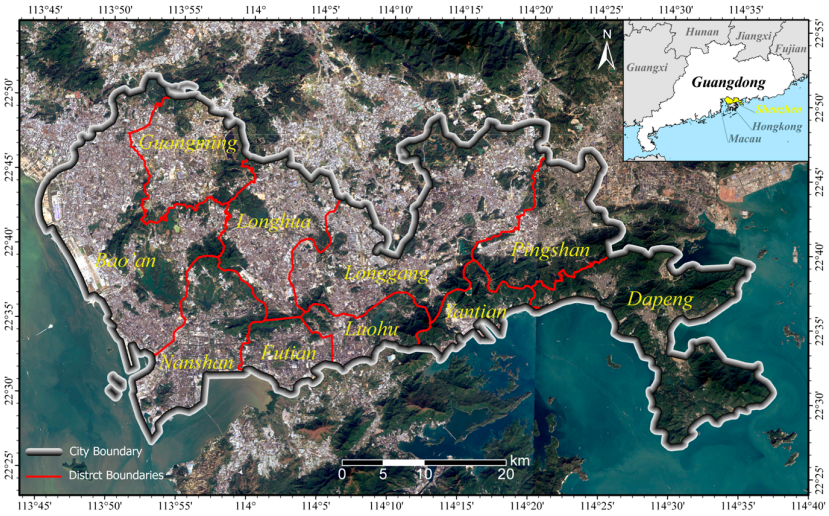

Figure 1. Study area.

The Typical Meteorological Year (TMYx) data covering the period 2009 to 2015, together with the actual meteorological year (AMY) data for 2020, used in this study were obtained from Oikolab (oikolab.com). Building vector data for Shenzhen were obtained from the Global Building Atlas[16]. Building function classifications and other attribute information were extracted from Open Street Map point-of-interest data, while building height information was derived from the Chinese Building Height dataset at 10 m spatial resolution [17].

2.2. Methods

The study first performs physics-based simulations to estimate the energy consumption of typical residential buildings in Shenzhen. Based on these simulations, machine learning models are trained using meteorological variables, building geometric parameters, and temporal features to estimate the daily energy consumption of residential buildings across the entire city. The resulting energy consumption estimates are then used as spatial proxy data for bottom-up spatial allocation, enabling the estimation of CO_2 emissions from residential buildings throughout Shenzhen.

2.2.1. Physics-Based Modelling and Simulation

The selection of typical buildings, the specification of envelope constructions, and the definition of occupant-related disturbances are key determinants of the accuracy of building energy consumption simulations performed using EnergyPlus. To ensure that the model inputs accurately reflect local building characteristics, a comprehensive on-site survey was conducted in Shenzhen at the end of 2023, covering major residential areas across multiple districts, including Luohu, Futian, Nanshan, Bao'an, Longgang, and others. Based on the findings of field surveys, we classified residential buildings into five representative types, considering factors such as architectural form, mixed-use functions and construction period, as illustrated in Figure 2.

 doi:10.20944/preprints202603.1914.v1

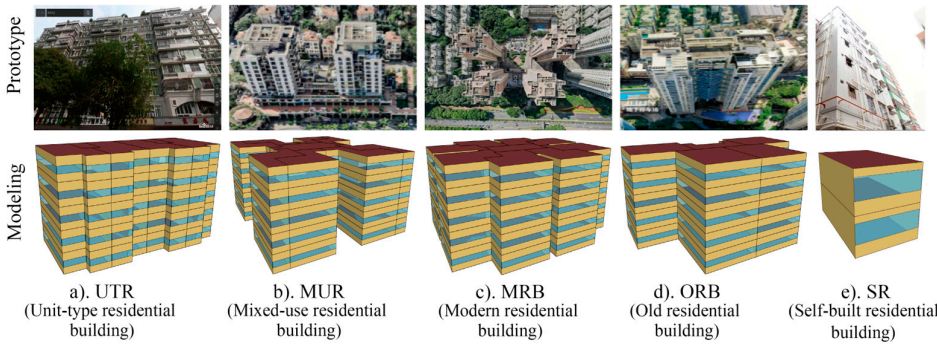

Figure 2. Prototype and modelling of typical residential building in Shenzhen.

Widely constructed between the 1980s and 2000s, UTR represents a distinctive urban residential typology characterised by modular, symmetrically arranged units with flexible layouts and predominantly north–south orientation. MUR represents a typical mixed-use residential form in southern Chinese cities, characterised by commercial uses on lower floors and residential units above. MRB and ORB are primarily residential in nature. Most ORB were constructed after the 1990s, whereas MRB represent more recent and modern architectural configurations. SR represents a typical self-built residential type commonly found in urban villages across southern China. The buildings are characterized by extremely high density and narrow spacing—often referred to as "handshake buildings"—with natural lighting primarily provided by the street-facing façade.

The specification of building envelope parameters followed the settings for the "hot summer and warm winter Zone B" defined in the national industry standard General Code for Energy Efficiency and Renewable Energy Utilization in Buildings (GB 55015-2021), complemented by findings from previous studies in relevant regions. In total, 336 valid questionnaires were collected during the field survey, comprising 116 paper-based responses and 220 online submissions. These data provide valuable insights into residential conditions and occupant living habits in Shenzhen. Combining the GB 55015 standard with relevant local codes for building simulation, a generalized occupant schedule was developed and used as the basis for modelling occupant-related disturbances.

The Open Studio was employed to develop three-dimensional models for the five typical building types. To enhance the generalisability of the simulation results, the internal spatial configurations were simplified, with each room represented as a single thermal zone (see Figure 2). Furthermore, a series of multi-storey models was batch-generated for different building types, ranging from single-storey structures to high-rise buildings of up to 33 floors, to support large-scale energy consumption simulations. A total of 126 building models was generated in this process.

The meteorological data utilised for Energy Plus simulations was sourced from the TMYx meteorological dataset provided by Oikolab for the Shenzhen International Meteorological Station (ID 594930). All simulations were conducted with a daily time step, and the set-point temperature of the air-conditioning equipment was fixed at 26 °C, consistent with the operational mode identified from the preliminary survey data.

2.2.2. Machine Learning Models

Prior to model training, a systematic data quality control and preprocessing workflow was applied to the simulated building energy consumption outputs. Outliers in the daily energy use intensity (DEUI) dataset, accounting for 0.10% of the observations, were identified and excluded using the Z-score criterion ($|Z| \geq 3$). Subsequently, missing values were imputed by assigning the median DEUI value of the corresponding building type for the same calendar day.

Based on an in-depth examination of the statistical characteristics and physical interpretations of the source parameters, additional derived features were constructed to enhance the model's explanatory capacity. New engineering variables such as High duration, CDD, and day of year have been incorporated to capture both the climatic responsiveness and temporal periodicity of building

 doi:10.20944/preprints202603.1914.v1

energy consumption. The definitions and meanings of all feature parameters are summarised in Table A1.

A systematic feature selection procedure was implemented using feature importance measures and the correlation coefficient matrix. Figure A1 presents the visualization of feature importance and the correlation matrix. Feature selection was guided by two principles: (a) the selected features should encompass building, meteorological, and temporal feature clusters and sufficiently represent their key characteristics; and (b) among highly correlated variables, features with higher importance and greater data availability were prioritised. Accordingly, a final set of features—including Temp Mean, High duration, RH Mean, GHrad Sum, is weekend, doy sin, doy cos, Building Type, Building Area and Floor.

To capture the complex and nonlinear interactions among meteorological variables, building characteristics, and energy consumption, this study employed and systematically evaluated a series of machine learning algorithms. The models used include linear models such as Ridge, Lasso, and Elastic Net; bagging-based tree models such as Decision Tree and Random Forest; and boosting-based ensemble models including Gradient Boosting Machine (GBM), LightGBM, CatBoost, and XGBoost.

Since daily building energy consumption data exhibit strong temporal dependencies, the Time-Block partitioning strategy was employed to ensure that model evaluation accurately reflects the true performance of time-series data. In this method, the entire dataset was divided along the temporal axis into fixed-length training and testing blocks. In each fold, the training set includes all observations preceding the current testing period, while the testing set consists of the subsequent time segment. A schematic illustration of this procedure is provided in Figure A2. All building samples are synchronously partitioned across identical time intervals, ensuring that both training and testing blocks contain data from the same temporal span for all buildings and avoiding information leakage from future.

Based on the time-block partitioning strategy, the dataset was divided into multiple folds, and the average values of the evaluation metrics across folds were used to represent model performance under this partitioning scheme. To ensure the robustness and generalization capability of model evaluation, all models were tested under various combinations of training and testing window lengths. Specifically, the initial training window (TR) ranged from 28 to 182 days, with an increment of 7 days, while the testing window (T) varied from 7 to 28 days, also in 7-day increments. The performance of each model was comprehensively assessed using multiple evaluation metrics, including the coefficient of determination (R^2), root mean square error (RMSE), and mean absolute error (MAE).

2.2.3. Model Interpretation and Feature Contribution Analysis

Explainable machine learning models have attracted growing interest because they can quantify the contributory effects of individual features on model estimations, thereby improving transparency and interpretability. The theoretical foundation of the SHAP (SHapley Additive exPlanations) framework is rooted in the concept of Shapley values from cooperative game theory [18], which enables the equitable attribution of marginal contributions to each feature while adhering to the axioms of fairness and consistency.

The SHAP value for feature i, denoted as ϕ_i, is defined as the weighted average of the marginal contribution of feature i across all possible feature subsets S that do not include i:

$$\phi_i = \sum_{S \subseteq F \setminus \{i\}} \frac{|S|!\,(|F| - |S| - 1)!}{|F|!} [f(S \cup \{i\}) - f(S)] \quad (1)$$

where F represents the full set of input features, S denotes a subset of features excluding i, and $f(*)$ is the model output function.

Based on the SHAP framework, the output of a machine learning model for a given sample $x$can be expressed as an additive decomposition:

 doi:10.20944/preprints202603.1914.v1

$$f(x) = \phi_0 + \sum_{i=1}^{M} \phi_i \quad (2)$$

where ϕ_0 is the expected model output over the background dataset, and ϕ_i quantifies the contribution of the i-th feature to the deviation of the output from this baseline.

2.2.4. Model Estimation

Building energy consumption generally consists of two components: baseline load and occupant-related load. The baseline load refers to the energy consumed when the building is unoccupied, including standby equipment power, public lighting, server-room loads, and the basic operating load of HVAC systems. The occupant-related load varies with the number of occupants and their behavioural patterns. Without adjusting the simulation outputs for occupant density and occupancy rate, the full-occupancy assumption would inevitably lead to an overestimation of energy use [19,20]. Thus, modelling and correcting for occupancy and its associated factors is a critical step in aligning simulation results with real-world building performance.

We employ an Occupancy Intensity Coefficient to adjust the estimation results. This coefficient reflects the deviation of actual occupancy from the full-occupancy assumption and enables an appropriate correction of the occupant-related load component. The adjustment is calculated as follows:

$$E_{adj} = \beta E_{sim} + (1 - \beta) E_{sim} \cdot r \quad (3)$$

where E_{adj} denotes the adjusted energy consumption, and E_{sim} represents the simulated energy consumption estimated by the physical model. where r denotes the actual occupancy rate (i.e., the ratio of actual to design population), and β represents the proportion of baseline energy consumption.

The coefficient r is typically computed as the ratio of actual occupancy to design occupancy. The design occupancy is estimated using the building floor area divided by the per-capita floor area. According to the Sixth National Population Censuses, the per-capita floor area in Shenzhen is 27.8 m². The actual occupancy is determined from the WorldPop dataset by extracting the population counts within the spatial extent of each building.

Previous studies indicate that baseline loads typically account for 25–40% of total residential energy use [21], with higher fractions generally observed in commercial buildings. Questionnaire results further suggest that SR exhibit stronger energy-saving behaviour and own fewer basic appliances. Accordingly, baseline load proportions are set to 0.4 for MUR, 0.2 for SR, and 0.3 for other types. To reduce the influence of anomalous population values, the final adjustment coefficient is constrained to the range [0.2, 1.2].

2.2.5. Spatiotemporal Downscaling

The annual CO_2 emissions are accounted for using the inventory-based methodology recommended by the IPCC, which relies on sectoral statistical data. CO_2 emissions associated with energy consumption and industrial production processes are calculated according to inventory items disaggregated by sector and fuel type, together with their corresponding emission factors. The emissions are calculated using the following formula:

$$CE_{energy} = \sum_i \sum_j CE_{ij} = \sum_i \sum_j \left(AD_{ij} \times EF_j\right) \quad (4)$$

$$CE_{process} = \sum_t CE_t = \sum_t (AD_t \times EF_t) \quad (5)$$

where i represents the 47 industry sectors classified in the IPCC Guidelines, j stands for the 17 major types of fossil fuels as classified in the Guidelines. CE_{energy} represents CO_2 emissions of

 doi:10.20944/preprints202603.1914.v1

industry i from the combustion of energy source j, and $CE_{process}$ means the CO_2 emissions generated by the corresponding industrial process j. AD means the denotes the consumption of the corresponding energy source, and EF represents the CO_2 emission factor associated with that energy source.

To ensure consistency between estimated results and statistical records, downscaling methods were employed to disaggregate annual CO_2 emissions derived from statistical data into daily, building-level values. Using the adjusted building energy consumption values as weighting factors, daily building-level CO_2 emissions were computed accordingly, as follows:

$$CE_{ij} = CE_{total} \cdot \frac{EC_{ij}}{\sum EC_{ij}} \tag{6}$$

where CE_{ij} denotes the CO_2 emissions of building i on day j, CE_{total} represents the total annual CO_2 emissions of the building sector, and EC_{ij} denotes the adjusted building energy consumption value of building i on day j.

2.2.6. Validation

This study proposes two complementary validation approaches—one at the individual-building level and the other at the annual total emission level—to assess the plausibility and reliability of the model results.

At the individual building level, type-specific average energy intensity values were directly employed to derive building energy consumption estimates. Specifically, for the five typical building types, physics-based simulations were re-performed using the actual meteorological conditions of the target year. Building energy consumption was then derived using the average DEUI value for each building type together with the corresponding building floor area. Subsequently, 50 buildings were randomly selected from each category, yielding a sample of 250 buildings with complete annual energy consumption records. Model calibration and performance assessment were then performed at daily, monthly, and annual temporal scales, respectively.

Second, a validation was conducted from an aggregate perspective. Using the estimation energy consumption and the 2020 Guangdong provincial grid emission factor (0.445 kg CO_2/kWh), the annual total CO_2 emissions of Shenzhen's building sector for the year 2020 were estimated. This estimate was then compared against the building sector CO_2 emissions derived from official statistical data, enabling an assessment of the model's consistency and reliability at the city-wide scale.

The equation is formulated as:

$$CE_{total} = \sum EC_i \cdot EF \tag{7}$$

where EC_i denotes the annual total energy consumption of building i, EF represents the grid emission factor, and CE denotes the annual total CO_2 emissions of the building sector.

3. Results

3.1. Hybrid Model Results

3.1.1. Physics-Based Simulation Results

The green dashed line in Figure 3(a) represents the average DEUI variation across all building types. The energy use intensity of buildings exhibits pronounced seasonal and periodic patterns. The periodic variation is primarily manifested in the weekly cycle of DEUI, with residential buildings exhibiting higher DEUI on weekends than on weekdays. Regarding seasonality, Shenzhen has a subtropical monsoon climate characterised by hot summers and mild winters, with an extended period of high temperatures. The warming period typically begins in April and lasts until November, and temperatures seldom drop below 10 °C throughout the year. From early May to mid-October, the monthly average temperature remains above 25 °C for nearly half a year, leading to a significant increase in cooling demand and, consequently, higher DEUI.

 doi:10.20944/preprints202603.1914.v1

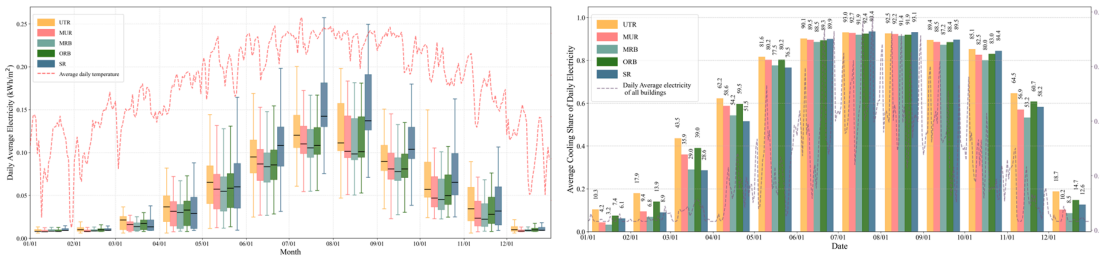

(**a**) (**b**)

Figure 3. (**a**) Typical building energy simulation results under TMY conditions; (**b**) Monthly variation in the share of cooling energy consumption in typical buildings.

The boxplots in Figure 3(a) illustrate the monthly distribution of DEUI across different building types. Both UTR and SR exhibit substantially higher DEUI levels compared with the other three categories. SR shows markedly larger median values, wider interquartile ranges, and more pronounced extremes. These differences become even more evident during the high-temperature period from May to October.

Figure 3(b) presents the average proportion of cooling energy consumption in the total daily energy use across different building types. During December, January, and February, cooling demand is minimal, and building energy use is primarily driven by equipment, lighting, and other non-cooling loads. As the average temperature rises, the share of cooling energy consumption increases steadily, reaching nearly 90% between June and September. This indicates that during the summer period, building energy use is dominated almost entirely by cooling demand.

3.1.2. ML Model Comparison

The R^2 performance of all models under different combinations of initial training and testing windows is illustrated in Figure 4. Different combinations of the initial training window and testing window have a considerable impact on the performance of the models. As the length of the initial training window increases, the overall performance of the models generally improves, although slight fluctuations can still be observed. The optimal performance of most models is achieved when the initial training window exceeds approximately 140 days, with a testing window of 21 or 28 days.

In terms of overall model performance, comparison of the average R^2 values indicates that the models with ensemble learning, such as GBM (0.739), CatBoost (0.735), and XGBoost (0.723), substantially outperforms the linear models Ridge, Elastic Net, and Lasso in this energy consumption estimation task. This suggests that the relationship between the feature variables and building energy-use efficiency is far more complex than can be captured by linear formulations. In contrast, the performance of basic tree-based models such as Decision Tree and Random Forest is relatively modest, falling short of the estimation accuracy achieved by the ensemble approaches.

The CatBoost model achieves the best overall performance among all models and window configurations when using a training window of 182 days and a testing window of 21 days, yielding R^2 = 0.879, RMSE = 0.0092, and MAE = 0.00686. Considering both estimation accuracy and computational efficiency, CatBoost was ultimately selected as the final model for building-level daily energy consumption estimation.

 doi:10.20944/preprints202603.1914.v1

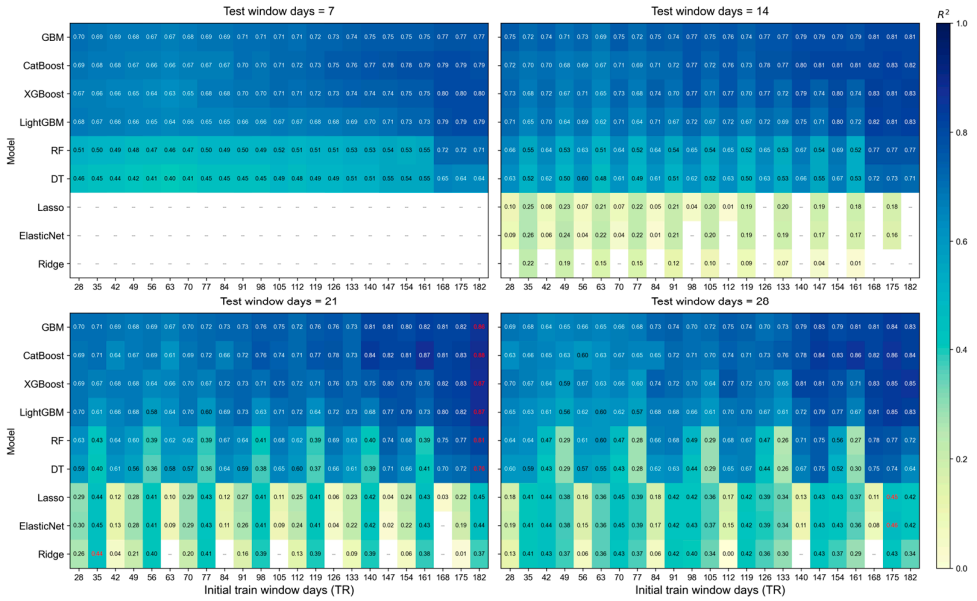

Figure 4. Comprehensive heatmap of model R^2 comparison (The blank areas in the figure indicate cases where the model performance is worse than that of the mean prediction baseline).

3.2. Feature Analysis

The SHAP summary beeswarm plot shows in Figure 5 illustrates the global feature contribution patterns of the model, addressing the question of which features are most important. The SHAP dependence plots for individual features further reveal the functional relationships between these key variables and energy consumption, explaining how each feature influences the estimation. Overall, meteorological variables constitute the primary drivers of the model's estimations, exerting substantially greater influence than temporal features and building physical attributes.

Daily mean temperature is identified as the most influential factor affecting final building energy consumption, followed by the duration of high-temperature conditions. Both features exhibit positive monotonic relationships and clear threshold effects. Specifically, when temperature or high-temperature duration exceeds certain critical values, the SHAP values rapidly become positive and increase significantly with further rises in temperature.

The impact of weekday–weekend consumption patterns on building energy use is more pronounced than that of seasonal variations. Significant differences are observed between weekends and weekdays: weekends tend to increase building energy consumption, whereas weekdays generally suppress its growth.

Among building types, UTR and SR buildings are associated with increased energy consumption, whereas the remaining building types exhibit a slight suppressing effect on energy use. The SHAP curve for building area shifts from positive to negative contributions, suggesting that smaller buildings tend to have higher daily electricity consumption, while the marginal effect diminishes as floor area increases. This likely reflects larger residential units having greater per-capita floor area, more shared or non-conditioned spaces, and cooling loads that do not scale proportionally with total floor area.

 doi:10.20944/preprints202603.1914.v1

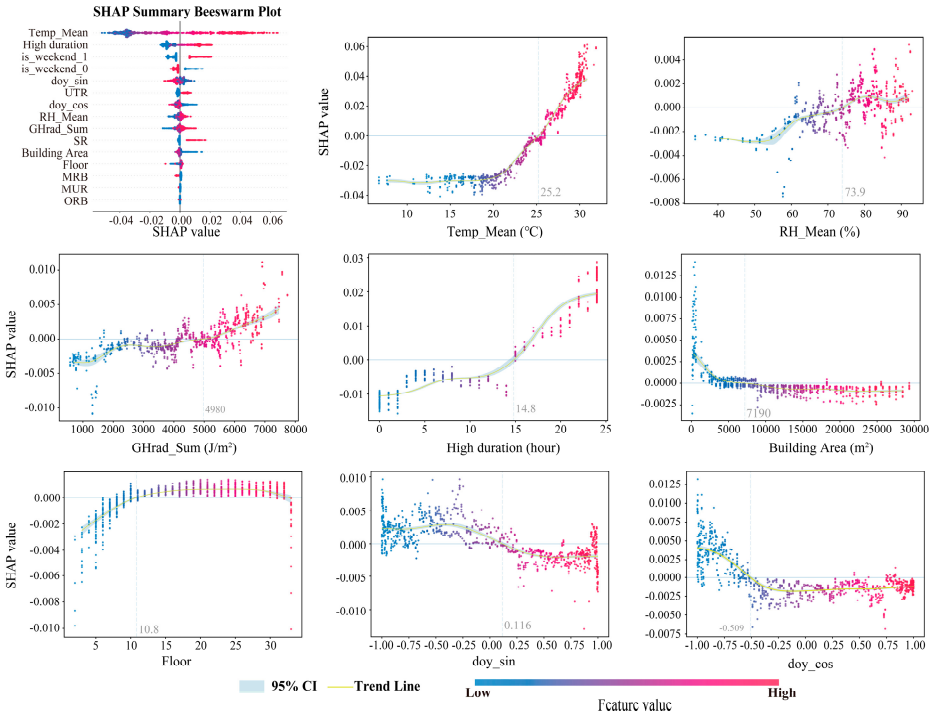

Figure 5. SHAP dependence plots for individual features.

In addition, global horizontal irradiance, relative humidity, and the number of floors all exhibit positive monotonic effects on building energy consumption.

3.3. Spatiotemporal Distribution

3.3.1. Total CO_2 Emissions by District

Figure 6 illustrates the spatiotemporal distribution of CO_2 emissions from the building sector in Shenzhen for the year 2020 following the downscaling correction. Areas with high building CO_2 emissions are predominantly concentrated in the central and southern districts of Shenzhen, including Longhua, Luohu, Bao'an, Nanshan, and Futian. This spatial pattern is consistent with the distribution of high-emission buildings—defined as those emitting more than 50 tonnes of CO_2 annually—across these districts, as illustrated by the pie chart in Figure 6.

Moreover, a notable spatial pattern can be observed in the enlarged sub-maps a, b and c in Figure 6: buildings with relatively high CO_2 emissions are predominantly distributed along block perimeters adjacent to roads, whereas buildings located within block interiors generally exhibit lower emission levels. This pattern is consistently observed across all districts of Shenzhen. The underlying reason is that locations near roads typically benefit from better natural lighting conditions and greater transport accessibility than interior areas. As a result, buildings situated along block perimeters often have taller storeys and larger functional intensity, leading to higher CO_2 emission levels, even when the DEUI remains comparable. The finding suggests that targeted and fine-grained monitoring of street-front buildings within high-emission clusters is crucial for effectively controlling and reducing urban CO_2 emissions.

 doi:10.20944/preprints202603.1914.v1

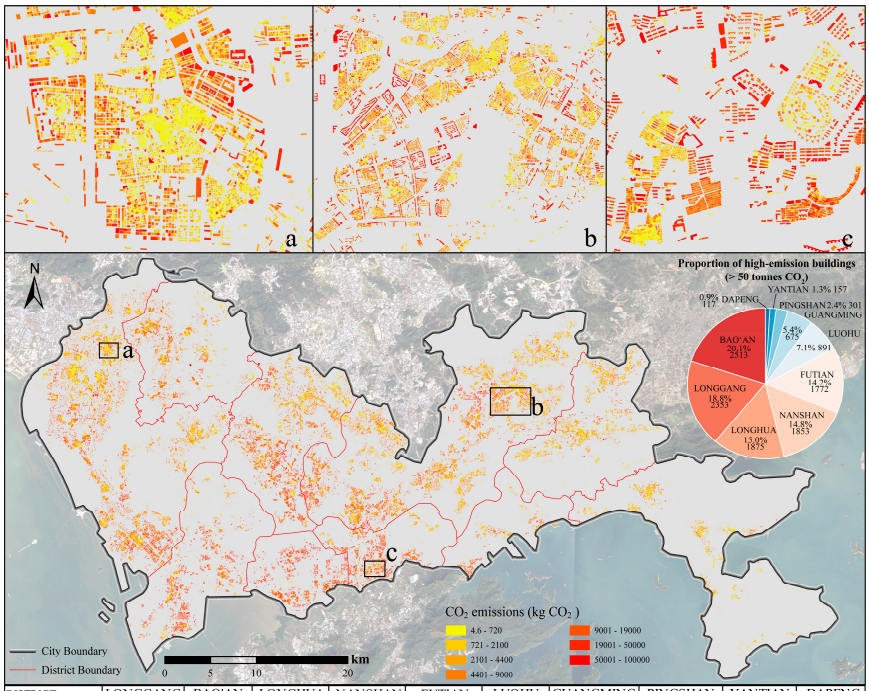

DISTRICT	LONGGANG	BAO'AN	LONGHUA	NANSHAN	FUTIAN	LUOHU	GUANGMING	PINGSHAN	YANTIAN	DAPENG
ANNUAL EMISSIONS 10^6 tonnes CO_2	111.9	95.4	72.0	62.9	56.0	37.8	30.3	17.6	6.7	5.4

Figure 6. Spatiotemporal patterns of building CO_2 emissions in Shenzhen, 2020.

The table at the bottom of Figure 6 presents the emission data for each district in Shenzhen for the year 2020. Longgang District exhibits the highest annual building-related CO_2 emissions, followed by Bao'an, Longhua, Nanshan, and Futian. Annual emissions in Longgang reached 1.119 million tonnes of CO_2, accounting for 22.6% of the city's total, while emissions in Bao'an also exceeded 0.954 million tonnes of CO_2. In contrast, the lowest building CO_2 emissions were observed in Yantian (0.067 million tonnes of CO_2) and Dapeng (0.054 million tonnes of CO_2). This spatial pattern of emissions is broadly consistent with the total floor area of each district (as shown in Figure 7) and the distribution of population density across districts. In 2020, Bao'an recorded the largest permanent resident population (4.491 million), followed by Longgang (3.999 million) and Longhua (2.543 million).

3.3.2. CO_2 Emission Variations Across Building Types

Figure 7 illustrates the number and total floor area of different residential building types across districts. In terms of total building count, Longgang District ranks highest with 116,388 residential buildings, and also records the largest total floor area of 2,356.05 km². This is followed by Bao'an District, which has 109,077 residential buildings with a total floor area of 1,756.03 km².

Among different building types, MRB and SR buildings dominate in both quantity and total floor area. Across the entire city, there are 341,937 SR buildings with a total floor area of 3,122.34 km², and 36,311 MRB buildings with a total floor area of 3,733.82 km². Although SR buildings are far more numerous, they are typically low-rise with smaller footprints. In contrast, MRB buildings generally have greater heights and larger floor areas, resulting in a higher total floor area despite having nearly an order of magnitude fewer buildings than SR types.

Figure 8 presents the daily variation in total carbon emissions across different building types for each district in 2020. The temporal fluctuation patterns of emissions are broadly consistent among building types, with differences primarily reflected in their magnitudes. A pronounced increase in emissions is observed from May to October, corresponding to the extended high-temperature season in Shenzhen, during which cooling demand significantly increases and drives higher residential

 doi:10.20944/preprints202603.1914.v1

building emissions. Slight decreases are observed in June and August, while the peak emission period occurs from July to early August.

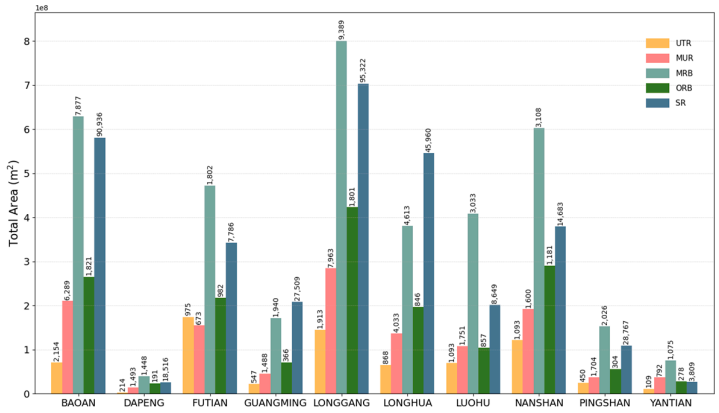

Figure 7. Total floor area by district and building type (The numbers at the top of the bar chart indicate the number of buildings).

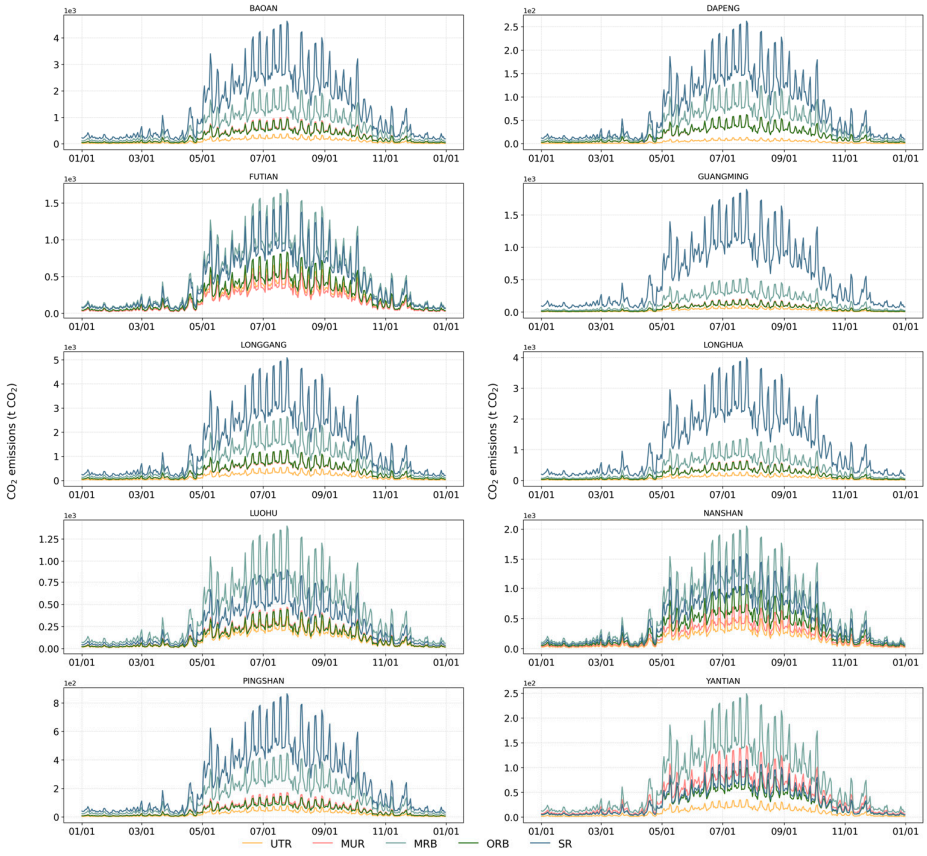

Figure 8. Trends in daily average CO_2 emissions by building type across districts.

In Guangming and Longhua districts, emissions are predominantly contributed by SR buildings. In Yantian District, MRB buildings account for the largest share of emissions, while SR buildings contribute relatively less. In Nanshan District, the contributions from different building types are more evenly distributed. In the remaining districts, MRB and SR buildings serve as the primary emission sources.

 doi:10.20944/preprints202603.1914.v1

These results are generally consistent with the distribution of building counts and total floor area, with MRB and SR buildings jointly contributing more than 50% of total carbon emissions in each district.

3.4. Validation

By fitting the model-estimated energy consumption against the reference values derived from specific building type average EUI, a consistently high level of agreement is observed across multiple temporal resolutions: the results for the 250-building sample are shown in Figure 9. At the daily scale, the overall R^2 value reached 0.970, with an RMSE of 0.011 tce. At the monthly scale, the R^2 value increased to 0.983, with an RMSE of 0.262 tce. At the annual scale, the R^2 value further improved to 0.987, with an RMSE of 2.305 tce. Collectively, these results indicate that the model exhibits strong robustness and reliability across different levels of temporal aggregation.

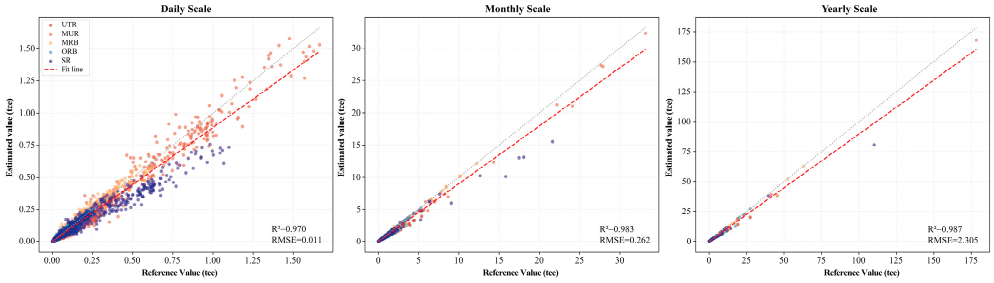

Figure 9. Fitting results at different scales.

At the building-type level, certain systematic deviations can be observed. For SR buildings, the model tends to slightly underestimate energy use compared with the reference values, whereas for MUR buildings, the estimations are generally higher than the corresponding benchmarks. Such discrepancies likely reflect underlying differences in internal loads, occupancy behaviours, or structural characteristics across building types, suggesting opportunities for further refinement of type-specific modelling components.

In the comparison of annual emission totals, the hybrid model estimates that CO_2 emissions from the building sector in Shenzhen in 2020 amount to 4.551 million tonnes, based on the grid emission factor. In contrast, the top-down statistical inventory reports 4.960 million tonnes. The absolute difference between the two estimates is approximately 0.484 million tonnes, corresponding to a relative error of 9.8%. It should be noted that the building energy consumption estimated by the hybrid framework only includes indirect energy use and does not account for direct energy consumption, such as natural gas. According to inventory estimates derived from statistical data, direct energy consumption in the building sector of Shenzhen in 2020 (e.g., natural gas) resulted in emissions of approximately 1.165 million tonnes of CO_2, which were directly incorporated into the final estimation results.

Due to differences in the statistical scope and completeness of activity data, as well as the use of local emission factors, discrepancies in urban CO_2 emission estimates among different inventories can range from 10% to 230% [22]. Moreover, this uncertainty generally increases as the spatial resolution becomes finer. Uncertainty analyses of high-resolution emission inventories in Europe have shown that the spatial disaggregation process alone may introduce approximately 40% uncertainty in CO_2 emissions [23]. Against this background, the level of discrepancy observed in this study is regarded as acceptable for city-scale building emission assessments, indicating that the proposed hybrid modelling framework exhibits reasonable reliability and applicability in estimating overall CO_2 emissions.

 doi:10.20944/preprints202603.1914.v1

4. Discussion

4.1. Distribution of High-Emission

To further investigate the differences in carbon emissions between road-adjacent buildings and those located within block interiors, OSM road network data were used to construct multi-level buffer zones based on road hierarchy. Buffer ranges of 0–100 m and 100–150 m were defined for primary roads; 0–60 m and 60–100 m for secondary roads; and 0–50 m and 50–75 m for tertiary roads. Carbon emissions of buildings located within these buffers were then quantified and compared across different road classes.

Table 1 presents the comparative results of building carbon emissions within the defined buffer zones. The results indicate that high-emission buildings are predominantly concentrated within the primary and secondary buffer zones, with the primary buffer zone containing up to 6,103 buildings, accounting for more than 44% of the total. Among different building types, ORB buildings exhibit the highest average per-building carbon emissions, reaching 7.49 tonnes in the primary buffer zone and 7.86 tonnes in the secondary buffer zone. In addition, ORB buildings within both buffer zones tend to have greater heights compared to other building types. Overall, buildings located within the primary and secondary buffer zones are generally taller than those situated outside the buffer zones.

Table 1. Comparative Statistics of Building Emissions within Buffer Zones.

Buffer zone	Building type	Building count of high emissions	Mean carbon emissions (t CO_2)	Mean building height (m)
Primary Buffer Zone	UTR	517	3.83	19.42
	MUR	658	2.33	12.01
	MRB	2024	4.35	19.91
	ORB	1009	7.49	28.71
	SR	1895	0.75	13.93
Secondary Buffer Zone	UTR	287	3.84	20.28
	MUR	270	3.27	12.80
	MRB	956	5.13	20.43
	ORB	540	7.86	28.93
	SR	1071	0.72	13.99
Outside the Buffer Zone	UTR	360	2.71	18.24
	MUR	353	1.21	10.75
	MRB	1397	2.55	16.38
	ORB	797	5.97	26.73
	SR	1604	0.51	12.37

From the perspective of building construction and site selection, road-adjacent locations generally exhibit superior natural lighting conditions and greater transport accessibility compared to interior areas. As a result, buildings situated along block perimeters often have taller stories and larger functional intensity, leading to higher CO_2 emission levels, even when the DEUI remains comparable. The finding suggests that targeted and fine-grained monitoring of street-front buildings within high-emission clusters is crucial for effectively controlling and reducing urban CO_2 emissions.

4.2. Comparison with Other Proxy Data

The spatialization of bottom-up carbon emission inventories derived from activity data is generally conducted through spatial downscaling based on spatial proxy data. Proxy data adopted in such studies often vary with the spatial scale of analysis. At the provincial or municipal scale, gross domestic product (GDP) and other economic indicators are frequently adopted, as CO_2 emission intensity is often strongly correlated with economic output. In contrast, fine-scale studies require more detailed spatial proxy data to enhance estimation accuracy and avoid spatial homogenization.

 doi:10.20944/preprints202603.1914.v1

Common fine-resolution proxies include population density, land-use and land-cover (LULC) data, and nighttime light (NTL) imagery. In certain contexts, datasets reflecting human activity intensity—such as mobile phone signalling records and taxi trajectory data—have also been employed for spatial allocation.

Population distribution data are usually derived from census-based statistics and reported at administrative-unit levels, limiting their applicability in fine-resolution analyses. Although land-cover datasets exhibit some correlation with CO_2 emission intensity, substantial within-class heterogeneity constrains their representativeness. Furthermore, most land-cover products lack sufficient temporal dynamics, and the assignment of weights across land-cover categories introduces additional uncertainty [24].

NTL data have been widely used in recent years to characterize the intensity of urban human activities [25]. The brightness of urban nighttime illumination is typically closely associated with the level of economic activity and has been extensively applied in studies analysing urban GDP and electricity consumption. NTL data are among the few proxy datasets that can support multi-scale analyses. Fine-resolution NTL products are suitable for fine-scale investigations, whereas at the provincial or municipal level, the total nighttime light intensity is commonly used as an aggregate indicator. The advantages of NTL data lie in their global coverage, accessibility, and their capability to support relatively continuous spatiotemporal analyses. However, several limitations remain in practical applications. First, saturation effects—particularly in datasets such as Defence Meteorological Satellite Program (DMSP) and Visible Infrared Imaging Radiometer Suite (VIIRS)—can lead to signal distortion in highly illuminated urban cores. Second, at fine spatial scales, the influence of street lighting cannot be neglected, as it may substantially interfere with the disaggregation of CO_2 emissions across specific industrial or sectoral categories [26].

The study employs a hybrid framework to estimate energy consumption in the building sector. Since building energy use directly reflects corresponding CO_2 emission intensity, building-unit-based estimates provide substantially finer spatial granularity than conventional NTL-derived proxies. This enables clearer differentiation of energy use and CO_2 emission disparities among individual buildings, facilitating the identification of key emission sources and supporting the development of differentiated mitigation strategies. Conceptually, the fine-resolution results generated by the hybrid framework exhibit stronger comparability to bottom-up emission inventories aggregated from point sources. Moreover, employing hybrid-model-based energy consumption estimates as proxy data circumvents challenges inherent in NTL-based approaches, including saturation effects and interference from street lighting in representing emission activity intensity.

4.3. Application

Previous studies on CO_2 emissions from the building sector at the city level have predominantly adopted a top-down approach. Typically beginning with statistical yearbooks, these studies construct emission inventories to estimate annual total emissions. Subsequently, spatial allocation indices are developed based on proxy variables, such as population and economic indicators, to perform downscaling procedures. While this approach is effective for coarse-scale estimation and analysis, it has limited capability in achieving higher precision. Moreover, the accuracy and robustness of spatial allocation relying on proxy variables remain subject to considerable uncertainty.

Building upon conventional top-down methodologies, this study develops a hybrid framework that integrates physics-based simulation with machine learning to estimate building energy consumption. By replacing the spatiotemporal decomposition of CO_2 emissions that traditionally relies on proxy variables such as socio-economic indicators, this framework substantially enhances the resolution and accuracy of spatiotemporal allocation of urban building CO_2 emissions. Fine-resolution spatiotemporal mapping of CO_2 emissions enables a refined characterization of the baseline CO_2 emission status of the urban building sector, offering important technical and data support for identifying major emission sources and informing differentiated carbon reduction policies.

 doi:10.20944/preprints202603.1914.v1

Moreover, building-level CO_2 emission estimates at fine spatiotemporal resolution provide essential data support for the integration of multi-source CO_2 emission information. For example, when cross-validated with city-wide panoramic mobile monitoring data, building-level emission estimates can impose explicit source constraints on street-level observations, thereby enhancing the interpretability and quantitative reliability of mobile monitoring analyses [27,28]. Conversely, the high spatiotemporal resolution CO_2 concentration data obtained from panoramic mobile monitoring can be used to inversely constrain and further refine building-scale emission estimates.

A key advantage of the framework lies in its extendibility. In the physical modelling component, the prototype of typical buildings can be flexibly adjusted to align with the geometric and envelope characteristics of buildings in other cities. Such modifications allow the simulation component to reflect local construction practices and material properties more accurately. Additionally, the TMY dataset employed in this study can be readily replaced by meteorological observations or TMY files corresponding to the target region, ensuring that the climatic inputs driving the simulations remain context appropriate.

The machine-learning estimation module further enhances the framework's adaptability; however, regional climatic variability introduces important challenges. The relationships between variables and energy-use patterns are inherently climate dependent and may shift considerably across different climatic zones [9]. For instance, in Shenzhen—located in a hot-summer–warm-winter climate—space-heating demand is negligible, meaning that the local model does not incorporate heating-related features. When applying the framework to regions with substantial heating loads or markedly different seasonal dynamics, feature re-selection and model retraining are essential to ensure that the output relationships remain valid. Without such adjustments, the transferability of the model may be limited and could lead to systematic biases.

4.4. Limitations and Improvements

The current study has several limitations, which are summarized as follows:

First, there are certain limitations in the selection of typical buildings and the specification of building envelope parameters. In general, typical buildings are selected based on regional representativeness and distinct architectural characteristics, yet there is no standardised or quantitative framework to guide this process, making the selection highly subjective. As a result, the chosen building types cannot fully represent all architectural forms within the study area but rather capture and generalise the most salient typological features. Similarly, although the building envelope parameters adopted in this study were referenced from relevant national technical standards, discrepancies still exist between the actual construction materials and the assumed specifications. Moreover, building envelope structures and materials vary across different construction periods, introducing additional uncertainty. Therefore, the selection of typical buildings and the specification of envelope parameters can only achieve approximate coverage of the overall building stock, which may lead to certain deviations in the simulated energy consumption results. Moreover, the moderate discrepancies observed for certain building types highlight the need for ongoing refinement of type-specific modelling components. Although the validation results at the citywide scale are generally satisfactory, differences in internal loads, occupancy behaviours, and functional characteristics across building types can lead to systematic deviations between estimated and reference values [29]. Incorporating more detailed behavioural or operational data—where available—may help address these discrepancies and improve model specificity.

Second, due to the limited availability of complete building energy consumption data and the severe lack of historical records, no building-level daily energy data covering an entire year were available for direct model validation. Therefore, an alternative approach was adopted: Re-estimating building energy consumption based on average EUI of typical buildings, which is considered relatively reliable at the monthly scale, and the resulting data were used as reference values for comparative validation. The comparative results exhibit good consistency, indicating that the estimates produced by the proposed framework are reasonably reliable and provide a more detailed

 doi:10.20944/preprints202603.1914.v1

differentiation of building energy consumption patterns. However, it remains uncertain which method more accurately reflects the actual conditions. Hence, future research should prioritise the collection of complete and reliable building energy consumption data to enable more rigorous model evaluation and validation.

Third, the results estimated by the hybrid modelling framework reflect indirect energy consumption and do not account for direct energy consumption. In the annual downscaling allocation of CO_2 emissions, it was assumed that indirect and direct energy consumption occur in equal proportions across all buildings. Accordingly, the results of CO_2 emissions generated by the model were directly used as weighting factors for spatiotemporal downscaling. This assumption may result in the overestimation of CO_2 emissions for buildings that do not rely on direct energy sources [25]. Future work should therefore consider treating direct energy consumption separately, to further improve the accuracy and robustness of the model outputs.

Finally, enhancing the model's transferability and applicability across different cities is essential [8]. The current model is primarily trained on buildings within a single climatic region, which limits its generalisability when applied to other climate zones. Future work may extend the framework to support multi-climate analysis by developing a standardised feature engineering and preprocessing system, establishing climate-zone-specific characteristic building libraries and corresponding submodules, and integrating multi-source datasets. These efforts would enable multi-city joint training and the development of a cross-regional energy estimation model with improved robustness and transferability.

5. Conclusions

This study proposes a hybrid modelling framework that integrates physics-based building energy consumption simulation with machine learning estimation to assess energy-related carbon emissions from residential buildings at the urban scale. This study employs estimated building energy consumption as a spatiotemporal proxy, replacing conventional variables used in traditional bottom-up approaches. Compared with commonly used proxy variables, the proposed framework significantly improves the spatiotemporal resolution and accuracy of urban CO_2 emission disaggregation. The CatBoost model is adopted to estimate residential building energy consumption at the city scale. Evaluation results demonstrate strong consistency of the estimated energy use across daily, monthly, and annual timescales, confirming the robustness and reliability of the approach.

Daily mean temperature and the duration of high-temperature conditions are identified as the primary drivers of daily energy consumption variability. Energy use exhibits pronounced periodic and seasonal patterns, with higher consumption observed on weekends compared to weekdays, and in summer relative to other seasons. The relative error between the estimated annual emissions and statistical benchmarks falls within an acceptable range for city-scale studies, indicating the method's applicability for emission inventory development and policy assessment. Spatially, carbon emissions in Shenzhen in 2020 are concentrated in the central and western districts, with Longgang recording the highest emissions (11.19 Mt), followed by Bao'an, Longhua, and Nanshan. High-emission buildings are mainly distributed along road-adjacent areas, predominantly consisting of ORB-type buildings.

Overall, the proposed hybrid modelling framework offers a robust, flexible, and interpretable approach for urban building energy and CO_2 assessment. The application of the proposed framework helps city administrators and policymakers better understand the fundamental characteristics of urban building CO_2 emissions, providing a robust analytical basis for clarifying emission responsibilities and supporting the formulation of targeted carbon reduction and energy-efficiency strategies, while also facilitating future research on data-driven urban energy systems.

Author Contributions: Conceptualization, L.Y. and L.W.; methodology, L.Y., Y.Z., K.W. and L.W.; software, L.Y., Y.Z.; validation, L.Y.; formal analysis, L.Y.; investigation, L.Y., Y.Z., K.W. and L.W.; resources, B.H., Z.N. and L.W.; data curation, L.Y., Y.Z. and K.W.; writing—original draft preparation, L.Y.; writing—review and

 doi:10.20944/preprints202603.1914.v1

editing, Y.Z. and L.W.; visualization, L.Y.; supervision, B.H., Z.N. and L.W.; project administration, B.H., Z.N. and L.W.; funding acquisition, Y.Z., K.W. and B.H. All authors have read and agreed to the published version of the manuscript.

Funding: This research was funded by the National Key Research and Development Program of China, grant number 2022YFB3903700, the Quantitative Study on the Ecological and Environment Impacts of Forest and Grassland in the Development Areas of Guohua Investment New Energy Projects, grant number CEZB240012576, the National Natural Science Foundation of China, grant number 42401558, the National Natural Science Foundation of China, grant number 42301340 and the Fundamental Research Funds for the Central Universities, grant number 590125071.

Data Availability Statement: The data that support the findings of this study are partially available from the corresponding author upon reasonable request.

Acknowledgments: All authors thank the anonymous reviewers and the editors for constructive comments that helped improve the manuscript.

Conflicts of Interest: The authors declare no conflicts of interest.

Abbreviations

The following abbreviations are used in this manuscript:

CO_2	Carbon dioxide
EUI	Energy use intensity
DEUI	Daily energy use intensity
TMY	Typical meteorological year
AMY	Actual meteorological year

Appendix A

Appendix A.1

Supplementary materials on feature selection and model training in machine learning.

Table A1. Descriptions of selected feature parameters

Feature type	Feature name	Description
Building morphology	Building Type	types of the five typical building types
	Floor	number of floors in the building
	Building Area	total floor area of the building
	Surface Area	surface area of the building
	Height	total height of the building
	Volume	total volume of the building
Meteorological	Temp_Mean & Tempa & Temp_min	the average, maximum and minimum daily temperatures
	RH_Mean	daily mean relative humidity
	WSpeed_Mean	daily average wind speed
	GHrad_Sum	daily sum of global horizontal radiation
	High duration	number of hours exceeding 26 ℃ per day
	CDD	cooling degree days based on 26 ℃ threshold
Temporal	month	representing seasonal effects
	day_of_year & doy_sin & doy_cos	sine and cosine transformations of day of year, representing seasonal effects
	is_weekend	to reflect differences between weekdays and weekends.
	weekday	to characterise weekly energy-use cycles.

 doi:10.20944/preprints202603.1914.v1

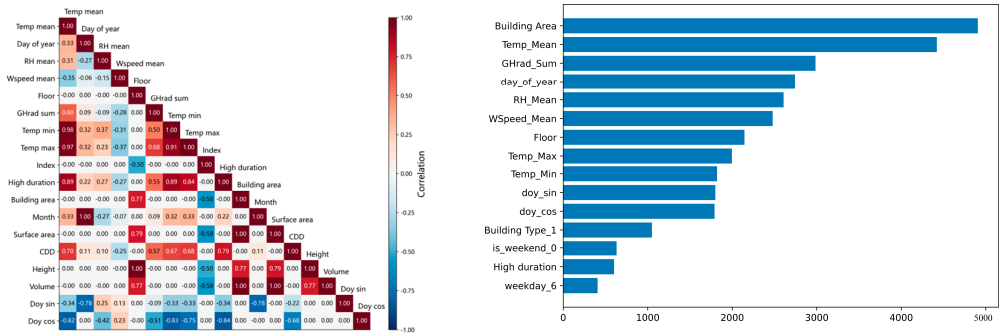

(**a**) (**b**)

Figure A1. (**a**) Feature correlation matrix heatmap; (**b**) Top 15 feature importances values (based on LightGBM native).

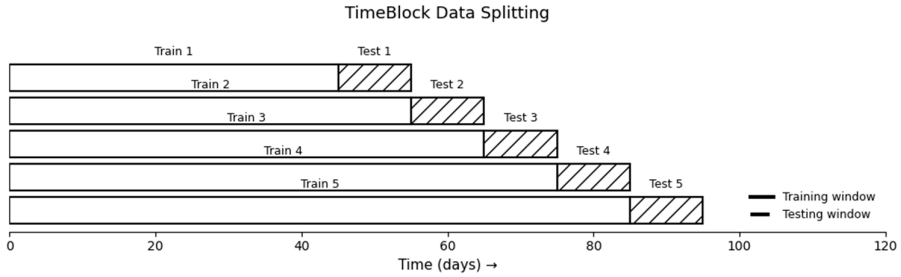

Figure A2. Schematic Diagram of Time-Block data splitting.

References

1. China Association of Building Energy Efficiency, Building Energy and Carbon Emissions Data Committee *Research Report on Carbon Emissions in the Field of Urban and Rural Development in China (2024 Edition)*; China Association of Building Energy Efficiency: Chongqing, 2024.
2. Tao, S.; Ru, M.Y.; Du, W.; Zhu, X.; Zhong, Q.R.; Li, B.G.; Shen, G.F.; Pan, X.L.; Meng, W.J.; Chen, Y.L.; et al. Quantifying the Rural Residential Energy Transition in China from 1992 to 2012 through a Representative National Survey. *Nat. Energy* **2018**, *3*, 567–573, doi:10.1038/s41560-018-0158-4.
3. Huo, T.; Ma, Y.; Cai, W.; Liu, B.; Mu, L. Will the Urbanization Process Influence the Peak of Carbon Emissions in the Building Sector? A Dynamic Scenario Simulation. *Energy Build.* **2021**, *232*, 110590, doi:10.1016/j.enbuild.2020.110590.
4. Fenner, A.E.; Kibert, C.J.; Woo, J.; Morque, S.; Razkenari, M.; Hakim, H.; Lu, X. The Carbon Footprint of Buildings: A Review of Methodologies and Applications. *Renew. Sustain. Energy Rev.* **2018**, *94*, 1142–1152, doi:10.1016/j.rser.2018.07.012.
5. Liu, Z.; Wang, F.; Tang, Z.; Tang, J. Predictions and Driving Factors of Production-Based CO2 Emissions in Beijing, China. *Sustain. Cities Soc.* **2020**, *53*, 101909, doi:10.1016/j.scs.2019.101909.
6. Chen, B.; Chen, F.; Ciais, P.; Zhang, H.; Lü, H.; Wang, T.; Chevallier, F.; Liu, Z.; Yuan, W.; Peters, W. Challenges to Achieve Carbon Neutrality of China by 2060: Status and Perspectives. *Sci. Bull.* **2022**, *67*, 2030–2035, doi:10.1016/j.scib.2022.08.025.
7. Huo, T.; Ren, H.; Zhang, X.; Cai, W.; Feng, W.; Zhou, N.; Wang, X. China's Energy Consumption in the Building Sector: A Statistical Yearbook-Energy Balance Sheet Based Splitting Method. *J. Clean. Prod.* **2018**, *185*, 665–679, doi:10.1016/j.jclepro.2018.02.283.
8. Khalil, M.; McGough, A.S.; Pourmirza, Z.; Pazhoohesh, M.; Walker, S. Machine Learning, Deep Learning and Statistical Analysis for Forecasting Building Energy Consumption — A Systematic Review. *Eng. Appl. Artif. Intell.* **2022**, *115*, 105287, doi:10.1016/j.engappai.2022.105287.
9. Xu, P.; Huang, J.; Shen, P.; Ma, X.; Gao, X.; Xu, Q.; Jiang, H.; Xiang, Y. Commercial Building Energy Use in Six Cities in Southern China. *Energy Policy* **2013**, *53*, 76–89, doi:10.1016/j.enpol.2012.10.002.

 doi:10.20944/preprints202603.1914.v1

10. IPCC *Climate Change 2023: Synthesis Report. Contribution of Working Groups I, II and III to the Sixth Assessment Report of the Intergovernmental Panel on Climate Change [Core Writing Team, H. Lee and J. Romero (Eds.)]*; IPCC: Geneva, Switzerland., 2023; p. 184;.
11. Muntean, M.; Janssens-Maenhout, G.; Song, S.; Giang, A.; Selin, N.E.; Zhong, H.; Zhao, Y.; Olivier, J.G.J.; Guizzardi, D.; Crippa, M.; et al. Evaluating EDGARv4.Tox2 Speciated Mercury Emissions Ex-Post Scenarios and Their Impacts on Modelled Global and Regional Wet Deposition Patterns. *Atmos. Environ.* **2018**, *184*, 56–68, doi:10.1016/j.atmosenv.2018.04.017.
12. Oda, T.; Maksyutov, S.; Andres, R.J. The Open-Source Data Inventory for Anthropogenic CO_2 , Version 2016 (ODIAC2016): A Global Monthly Fossil Fuel CO_2 Gridded Emissions Data Product for Tracer Transport Simulations and Surface Flux Inversions. *Earth Syst. Sci. Data* **2018**, *10*, 87–107, doi:10.5194/essd-10-87-2018.
13. Ramos, P.V.B.; Villela, S.M.; Silva, W.N.; Dias, B.H. Residential Energy Consumption Forecasting Using Deep Learning Models. *Appl. Energy* **2023**, *350*, 121705, doi:10.1016/j.apenergy.2023.121705.
14. Chen, S.; Li, N.; Guan, J.; Xie, Y.; Sun, F.; Ni, J. A Statistical Method to Investigate National Energy Consumption in the Residential Building Sector of China. *Energy Build.* **2008**, *40*, 654–665, doi:10.1016/j.enbuild.2007.04.022.
15. Cui, X.; Lee, M.; Koo, C.; Hong, T. Energy Consumption Prediction and Household Feature Analysis for Different Residential Building Types Using Machine Learning and SHAP: Toward Energy-Efficient Buildings. *Energy Build.* **2024**, *309*, 113997, doi:10.1016/j.enbuild.2024.113997.
16. Zhu, X.X.; Chen, S.; Zhang, F.; Shi, Y.; Wang, Y. Global Building Atlas: An Open Global and Complete Dataset of Building Polygons, Heights and LoD1 3D Models. *Earth Syst. Sci. Data* **2025**, *17*, 6647–6668, doi:10.5194/essd-17-6647-2025.
17. Wu, W.-B.; Ma, J.; Banzhaf, E.; Meadows, M.E.; Yu, Z.-W.; Guo, F.-X.; Sengupta, D.; Cai, X.-X.; Zhao, B. A First Chinese Building Height Estimate at 10 m Resolution (CNBH-10 m) Using Multi-Source Earth Observations and Machine Learning. *Remote Sens. Environ.* **2023**, *291*, 113578, doi:10.1016/j.rse.2023.113578.
18. Lundberg, S.M.; Lee, S.-I. A Unified Approach to Interpreting Model Predictions. In Proceedings of the ADVANCES IN NEURAL INFORMATION PROCESSING SYSTEMS 30 (NIPS 2017); Guyon, I., Luxburg, U.V., Bengio, S., Wallach, H., Fergus, R., Vishwanathan, S., Garnett, R., Eds.; Neural Information Processing Systems (nips): Long Beach, CA, 2017; Vol. 30.
19. Li, J.; Yu, Z. (Jerry); Haghighat, F.; Zhang, G. Development and Improvement of Occupant Behavior Models towards Realistic Building Performance Simulation: A Review. *Sustain. Cities Soc.* **2019**, *50*, 101685, doi:10.1016/j.scs.2019.101685.
20. Peng, Y.; Rysanek, A.; Nagy, Z.; Schlüter, A. Using Machine Learning Techniques for Occupancy-Prediction-Based Cooling Control in Office Buildings. *Appl. Energy* **2018**, *211*, 1343–1358, doi:10.1016/j.apenergy.2017.12.002.
21. Liang, X.; Hong, T.; Shen, G.Q. Improving the Accuracy of Energy Baseline Models for Commercial Buildings with Occupancy Data. *Appl. Energy* **2016**, *179*, 247–260, doi:10.1016/j.apenergy.2016.06.141.
22. Tao, M.; Cai, Z.; Che, K.; Liu, Y.; Yang, D.; Wu, L.; Wang, P.; Yang, M. Cross-Inventory Uncertainty Analysis of Fossil Fuel CO2 Emissions for Prefecture-Level Cities in Shandong Province. *Atmosphere* **2022**, *13*, 1474, doi:10.3390/atmos13091474.
23. Super, I.; Dellaert, S.N.C.; Visschedijk, A.J.H.; Denier Van Der Gon, H.A.C. Uncertainty Analysis of a European High-Resolution Emission Inventory of CO_2 and CO to Support Inverse Modelling and Network Design. *Atmospheric Chem. Phys.* **2020**, *20*, 1795–1816, doi:10.5194/acp-20-1795-2020.
24. Zhang, Y.; Sun, T.; Wang, L.; Huang, B.; Pan, X.; Song, W.; Wang, K.; Xiong, X.; Xu, S.; Yao, L.; et al. Portraying On-Road CO2 Concentrations Using Street View Panoramas and Ensemble Learning. *Sci. Total Environ.* **2024**, *946*, 174326, doi:10.1016/j.scitotenv.2024.174326.
25. Liu, G.; Zheng, Y.; Xu, X.; Liu, X.; Zhang, H.; Ou, J. Fine-Scale Estimation of Building Operation Carbon Emissions: A Case Study of the Pearl River Delta Urban Agglomeration. *Build. Simul.* **2025**, *18*, 957–977, doi:10.1007/s12273-025-1265-3.

 doi:10.20944/preprints202603.1914.v1

26. Yin, Z.; Chen, F.; Dou, C.; Wu, M.; Niu, Z.; Wang, L.; Xu, S. Identification of Illumination Source Types Using Nighttime Light Images from SDGSAT-1. *Int. J. Digit. Earth* **2024**, *17*, 2297013, doi:10.1080/17538947.2023.2297013.
27. Fong, W.; Sun, Y.; Chen, Y. Examining the Relationship between Energy Consumption and Unfavorable CO2 Emissions on Sustainable Development by Going through Various Violated Factors and Stochastic Disturbance–Based on a Three-Stage SBM-DEA Model. *Energies* **2022**, *15*, 569, doi:10.3390/en15020569.
28. Zhang, Y.; Sun, T.; Wang, L.; Huang, B.; Xu, S.; Pan, X.; Xiong, X.; Song, W.; Li, G.; Niu, Z. Integrating Panoptic-AI and Multi-Source Observations for Daytime Dynamic CO2 Increment Prediction in Urban Traffic Networks. *Sustain. Cities Soc.* **2025**, *131*, 106730, doi:10.1016/j.scs.2025.106730.
29. Reinhart, C.F.; Cerezo Davila, C. Urban Building Energy Modeling – A Review of a Nascent Field. *Build. Environ.* **2016**, *97*, 196–202, doi:10.1016/j.buildenv.2015.12.001.